Materials Today Bio 26 (2024) 101075

Contents lists available at ScienceDirect

Materials Today Bio

journal homepage: www.journals.elsevier.com/materials-today-bio

CuCS/Cur composite wound dressings promote neuralized skin regeneration by rebuilding the nerve cell "factory" in deep skin burns

Zhaowenbin Zhang [a,b,c,1], Di Chang [a,b,c,d,1], Zhen Zeng [a,b,c,e,f,1], Yuze Xu [c], Jing Yu [a,b,c], Chen Fan [a,b,c], Chen Yang [a,b,c,**], Jiang Chang [a,b,c,*]

[a] Joint Centre of Translational Medicine, The First Affiliated Hospital of Wenzhou Medical University, Wenzhou, 325000, People's Republic of China
[b] Zhejiang Engineering Research Center for Tissue Repair Materials, Wenzhou Institute, University of Chinese Academy of Sciences, Wenzhou, 325000, People's Republic of China
[c] State Key Laboratory of High-Performance Ceramics and Superfine Microstructure, Shanghai Institute of Ceramics, Chinese Academy of Sciences, Shanghai, 200050, People's Republic of China
[d] Fudan University, Shanghai, 200433, People's Republic of China
[e] Key Laboratory of Rehabilitation Medicine in Sichuan Province, West China Hospital, Sichuan University, Chengdu, People's Republic of China
[f] The Second Affiliated Hospital of Wenzhou Medical University, Wenzhou, Zhejiang, 325000, People's Republic of China

ARTICLE INFO

Keywords:
Burn wound healing
Cu^{2+} and Cur chelate
Neural network regeneration
Hair follicle regeneration

ABSTRACT

Regenerating skin nerves in deep burn wounds poses a significant clinical challenge. In this study, we designed an electrospun wound dressing called CuCS/Cur, which incorporates copper-doped calcium silicate (CuCS) and curcumin (Cur). The unique wound dressing releases a bioactive Cu^{2+}-Cur chelate that plays a crucial role in addressing this challenge. By rebuilding the "factory" (hair follicle) responsible for producing nerve cells, CuCS/Cur induces a high expression of nerve-related factors within the hair follicle cells and promotes an abundant source of nerves for burn wounds. Moreover, the Cu^{2+}-Cur chelate activates the differentiation of nerve cells into a mature nerve cell network, thereby efficiently promoting the reconstruction of the neural network in burn wounds. Additionally, the Cu^{2+}-Cur chelate significantly stimulates angiogenesis in the burn area, ensuring ample nutrients for burn wound repair, hair follicle regeneration, and nerve regeneration. This study confirms the crucial role of chelation synergy between bioactive ions and flavonoids in promoting the regeneration of neuralized skin through wound dressings, providing valuable insights for the development of new biomaterials aimed at enhancing neural repair.

1. Introduction

The integumentary system, recognized for its pronounced sensitivity, teems with a diverse array of nerve terminals that discern between noxious stimuli, thermal variations, and tactile sensations. Devastatingly, severe thermal injuries risk impairing these cutaneous nerves, and their associated sensory bodies, a damage that may progress to enduring sensory dysfunction in the absence of swift remedial intervention [1–3]. The prevalent therapeutic modality for such severe burns predominantly targets the restoration of the dermal structure, with a conspicuous lack of effective strategies to reinstate the tactile perception of the skin [4–8]. This shortfall arises from the limitations of the existing wound repair materials that fail to stimulate neural regeneration during skin restoration effectively. Therefore, the exploration and development of innovative wound repair materials capable of encouraging cutaneous peripheral nerve regeneration during burn wound repair carry significant implications [9–11].

The regeneration of hair follicles of superior quality is a crucial requirement for cutaneous nerve regeneration during the healing process of burn wounds [2,12–15]. The underlying reason for this lies in the function of hair follicles as the primary reservoir for the provision of cells related to the skin's neural components, serving as specialized

* Corresponding author. Joint Centre of Translational Medicine, The First Affiliated Hospital of Wenzhou Medical University, Wenzhou, 325000, People's Republic of China.
** Corresponding author. Joint Centre of Translational Medicine, The First Affiliated Hospital of Wenzhou Medical University, Wenzhou, 325000, People's Republic of China.
E-mail addresses: cryangchen@ucas.ac.cn (C. Yang), jchang@mail.sic.ac.cn (J. Chang).
[1] Zhaowenbin Zhang, Di Chang, and Zhen Zeng contributed equally to this work.

https://doi.org/10.1016/j.mtbio.2024.101075
Received 20 February 2024; Received in revised form 15 April 2024; Accepted 27 April 2024
Available online 27 April 2024

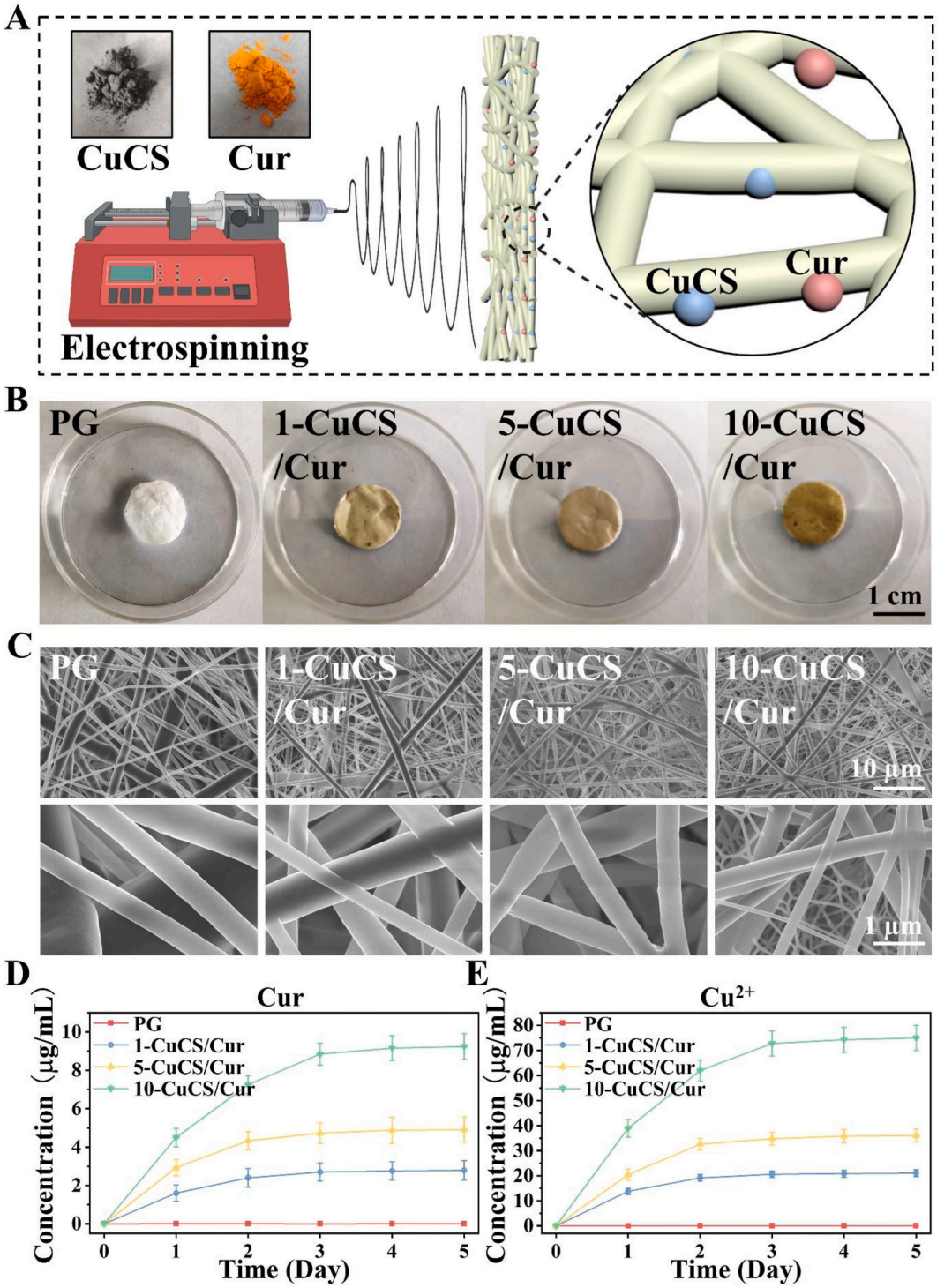

Fig. 1. Characterization of CuCS/Cur composite electrospun fiber membranes. (A) Schematic illustration of CuCS/Cur prepared by electrospinning. (B) Representative macrophotographs of CuCS/Cur. (C) Representative scanning electron microscope (SEM) images of CuCS/Cur. (D, E) Cur release performance and Cu^{2+} ion release performance of CuCS/Cur within 5 Days n = 6.

miniaturized organs that contribute the necessary cells for the growth of cutaneous nerves [16]. Also, severe burns may obliterate the hair follicles in the dermal layer of the wound area and cripple their activity along the wound's margin, thereby causing extensive harm to the skin's neural framework [1,17]. Additionally, burns often inflict significant vascular trauma, which hastens the apoptosis of compromised hair follicle tissues and hinders the regeneration of new hair follicles and rebuilding of neural networks [18]. Therefore, the quest for innovative wound repair materials capable of fostering simultaneous regeneration of hair follicles and blood vessels simultaneously might secure the secretion and translocation of nerve-related cells, thereby stimulating the restoration of the cutaneous sensory system during wound healing.

Within the realm of hair follicle regeneration, the utilization of hair follicle stem cells offers a direct and effective strategy. Nonetheless, its clinical application faces constraints due to challenges in controllability and elevated cost implications [19,20]. On the contrary, traditional

Chinese medicine extracts like curcumin (Cur, a type of flavonoid compound) are receiving increasing attention [21–24]. Evidence underpins that Cur encourages the secretion of auxin from hair follicles, inciting dormant hair follicle tissue to transition to the growth phase and hence prompting hair regeneration [8,25] However, Cur is an insoluble small molecule compound with low bioavailability, making it challenging to use directly [26]. Although prior studies have employed organic solvents such as dimethyl sulfoxide [27] or potent alkalis such as sodium hydroxide [28,29] to improve the solubility of Cur, these approaches do not favor wound healing [30]. Recent studies indicate that silicate bioceramics are able to release alkaline ions and create a mild alkaline microenvironment with a pH range between 8.5–9.5 [31]. This particular pH environment not only significantly stimulates fibroblast activity, thereby improving skin healing [32], but also enhances the dissolution of flavonoid compounds [33–35]. This characteristic potentially delineates a strategy to bolster the bioavailability of Cur in wound healing applications. Fascinatingly, silicate bioceramics also expedite vascularization during wound repair due to the sustained discharge of bioactive SiO_3^{2-} ions and other constituents [6,7,36]. For instance, our previous research demonstrated that copper-doped calcium silicate bioceramic (CuCS), which concurrently discharged Cu^{2+} and SiO_3^{2-} ions, enhanced vascularization during burn wound repair by inducing proliferation, migration of endothelial cells, and the expression of angiogenic growth factors like VEGF and HIF-1α [6]. Moreover, the released Cu^{2+} ions may further chelate with flavonoids to from Cu^{2+}--flavonoid chelates with potent biological activity. Cu^{2+}-quercetin chelates [6]. Given that Cur represents a typical flavonoid, it is hypothesized that CuCS may enhance the solubility of Cur, improve its bioavailability, and engender synergistic biological effects with Cur through potential Cu^{2+}-Cur chelates.

Based on the preceding analysis, we propose a wound dressing design incorporating CuCS and Cur in polymer matrix using electrospinning. Polycaprolactone (PCL) membranes are widely used as wound dressings because of their suitable mechanical property and biocompatibility, and the addition of gelatin during the process of electrospinning can further improve the hydrophilicity, degradability, and biofunctionality [37,38]. Therefore, we chose PCL and gelatin as polymer components to prepare the composite wound dressing. The operative principle of this dressing involves utilizing CuCS to create a mildly alkaline environment, thereby facilitating the dissolution of Cur. In tandem, Cu^{2+} ions are released to form chelates with Cur. The subsequent sustained delivery of Cu^{2+}-Cur chelate to the site of the burn wound fosters neural regeneration, chiefly through the expedited reparation of damaged hair follicles and blood vessels. To validate the aforementioned hypothesis, we introduced CuCS and Cur at diverse ratios into a commonly utilized electrospun wound dressing (Fig. 1A), aiming to optimize the release profile. Then, the efficacy of the CuCS/Cur wound dressing was evaluated in the context of burn wound healing and nerve regeneration using a mouse model with third-degree burns. Additionally, to substantiate the proposed biological mechanisms, a series of in vitro cell experiments were conducted, employing human hair follicle dermal papilla cells (HHDPCs), rat adrenal medulla pheochromoma differentiated cell line (PC12), and human umbilical vein endothelial cells (HUVECs).

2. Materials and methods

2.1. Materials

Tetraethyl orthosilicate (TEOS, CAS: 78-10-4), copper nitrate trihydrate ($Cu(NO_3)_2{\cdot}3H_2O$, CAS: 10031-43-3), calcium nitrate tetrahydrate ($Ca(NO_3)_2{\cdot}4H_2O$, CAS: 13477-34-4), copper chloride ($CuCl_2$, CAS: 10125-13-0), polycaprolactone (PCL, CAS: 24980-41-4), gelatin (CAS: 9000-70-8), hexafluoroisopropanol (CAS: 38701-74-5), acetic acid (CAS: 64-19-7), and curcumin (CAS: 458-37-7) were procured from Sinopharm Chemical Reagent Co., Ltd (Shanghai, China).

2.2. Preparation of copper-doped calcium silicate

Copper-doped calcium silicate (CuCS) was synthesized using a sol-gel method. The doping level of Cu was 5 mol% of Ca replaced by Cu. Initially, tetraethyl orthosilicate (TEOS) was hydrolyzed in deionized water, catalyzed by a 2 M HNO_3 solution, and stirred for 30 min. The molar ratio of TEOS, HNO_3, and H_2O was 1:0.16:8. Subsequently, $Ca(NO_3)_2{\cdot}4H_2O$ and $Cu(NO_3)_2{\cdot}3H_2O$ were added to the TEOS sols under continuous stirring, with a (Cu + Ca)/Si molar ratio of (0.05 + 0.95)/1. The reaction proceeded further under stirring conditions. Once the reaction was complete, the resulting sols were maintained at 60 °C for 24 h to form wet gels, which were then dried at 120 °C for 48 h to obtain xerogels. The xerogels were ground, sieved, and calcined at 800 °C. The CuCS powders were sieved again, and the particle size was reduced to less than 200 mesh.

2.3. Preparation of CuCS/Cur composite electrospun fiber membrane

Firstly, PCL/Gelatin (7:3) with a concentration of 10 % (w/v) was dissolved in a mixture of acetic acid and hexafluoroisopropanol (1:100). The solution is stirred for 24 h. Subsequently, CuCS and curcumin (Cur) are added to the solution, resulting in three variations named 1-CuCS/Cur, 5-CuCS/Cur, and 10-CuCS/Cur. The compositions for each variation are as follows: 1-CuCS/Cur: CuCS (1 mg), Cur (1 mg); 5-CuCS/Cur: CuCS (5 mg), Cur (5 mg); 10-CuCS/Cur: CuCS (10 mg), Cur (10 mg). After 30 min of sonication, the solution is further stirred for an additional 24 h. Next, the prepared solution is transferred into a 10 mL syringe for electrospinning. Electrospinning is carried out at a voltage of 15 kV with an injection rate of 0.02 mL/min, while keeping the collection distance between the needle tip and the rotating collector fixed at 15 cm. After 4 h, the resulting fibrous membranes are collected. The fiber membranes were stored in a vacuum oven at room temperature and subjected to a vacuum condition for 24 h to eliminate residual organic solvents [39,40]. The surface morphology of the composite films can be observed using a scanning electron microscope (SEM, S-4800, Hitachi, Japan).

2.4. Ion and drug release of CuCS/Cur composite fiber membrane

First, the standard curve of Cur was determined by taking the absorbance and Cur concentration in the range of 0–100 μg/mL as parameters, resulting in a correlation coefficient of $R^2 = 0.9996$. Next, the fiber membrane (100 mg) was added to 10 mL of phosphate-buffered saline (PBS, pH = 7.4) and shaken at 37 °C at 120 rpm. Subsequently, the solution of drug and ion release was collected at preset time points (Day 1, Day 2, Day 3, Day 4, and Day 5), and 10 mL of fresh PBS solution was added back. Finally, the collected solution was analyzed by UV/Vis spectroscopy to determine the concentration of Cur, and by ICP-AES (Thermo Fisher X Series 2, USA) to determine the concentration of Cu^{2+} ions.

2.5. Characterization of chelating ability of released products of CuCS/Cur

To evaluate the presence of a chelate in the release product of CuCS/Cur, the release product of CuCS/Cur was subjected to a 24-h immersion in 75 % ethanol, and the ultraviolet absorption spectrum was measured using a UV spectrophotometer. A control solution was prepared using a chelate of Cu^{2+} ions and Cur. The specific preparation steps for the Cu^{2+} ion and Cur chelate solution were as follows: First, 0.1 mmol (36.8 mg) of Cur was weighed and dissolved in 1 mL of DMSO. The solution was then diluted with 75 % ethanol to obtain a concentration of 0.050 μmol/mL. CuCl2 solutions (0.050 μmol/mL) were prepared using 75 % ethanol as the solvent. Then, Cu^{2+}-Cur chelate solutions were prepared by combining Cur solution with Cu^{2+} ions at a volume ratio of 1:1. Subsequently, the ultraviolet absorption spectrum was measured using a UV

spectrophotometer.

2.6. Cell culture

Human umbilical vein endothelial cells (HUVECs) were incubated in endothelial cell medium (ECM) (Sciencell, USA) supplemented with 5 % (vol/vol) fetal bovine serum (FBS) (Thermo Trace Ltd, Melbourne, Australia) and 1 % (vol/vol) endothelial cell growth supplement/heparin kit (ECGS/H) (Promocell). The medium for culturing human dermal fibroblasts (HDF) and rat adrenal medulla pheochromoma differentiated cell line (PC12) consisted of Dulbecco's Modified Eagle's Medium (DMEM) supplemented with 10 % fetal bovine serum (FBS) (Thermo Trace Ltd, Melbourne, Australia), 100 unit/mL penicillin, and 200 μg/mL streptomycin. Human hair follicle dermal papilla cells (HHDPCs) were cultured in mesenchymal stem cell medium (MSCM) (Sciencell, USA) supplemented with 5 % (vol/vol) fetal bovine serum (FBS) (Thermo Trace Ltd, Melbourne, Australia) and 1 % (vol/vol) mesenchymal stem cell growth supplement (MSCGS). It is worth mentioning that all cells used in this study were between passage 5 and 7.

2.7. Sterilization of CuCS/Cur composite fiber membrane

The electrospun fiber membrane was cut into a disc shape ($\Phi = 10$ mm). It was then placed in culture plates and sterilized using UV radiation. After being exposed to UV light for 1 h, the fibrous membrane was flipped over in a biosafety cabinet and subjected to an additional 1-h UV irradiation.

Effects of CuCS/Cur Composite Fiber Membrane on Cell Viability: The sterilized electrospun fiber membrane was placed in a 48-well culture plate. Next, HUVECs (5×10^3 cells/well) and HHDPCs (5×10^3 cells/well) were seeded onto the surface of the fiber membrane. The culture medium was replaced every other day. After 1, 3, and 5 days of culture, the cell viability of all samples was assessed by measuring the absorbance at 450 nm using a microplate reader with the CCK-8 assay.

2.8. Effects of CuCS/Cur composite fiber membrane on cell adhesion

The sterilized electrospun fiber membrane was placed in a 48-well culture plate. Subsequently, HUVECs (5×10^3/well) and HHDPCs (5×10^3/well) cells were seeded onto the surface of the fibrous membrane. The culture medium was replaced every other day. After 1 day of incubation, the fibrous membranes were washed with PBS and treated with 2.5 % glutaraldehyde for 40 min for fixation. Then, the cells were permeabilized with a 0.5 % TritonX-100 solution for 5 min. Following that, a prepared FITC phalloidin working solution (300 μL) was added to the fiber membrane, and the mixture was incubated in the dark at room temperature for 45 min. Finally, the nuclei were counterstained with a 200 μL DAPI solution. The stained fibrous membranes were observed using a confocal microscope (Leica TCS SP8).

2.9. The therapeutic effect of CuCS/Cur composite fiber membrane on deep burn

The animal procedures underwent review by the Experimental Animal Ethics Committee of the Animal Research and Ethics Committee of Wenzhou Institute of University of Chinese Academy of Sciences (WIUCAS23062718), ensuring compliance with national principles of animal protection, animal welfare, and ethics. Thirty 6-week-old female BALB/c mice were allocated into 5 groups, namely the blank group (Blank), pure fiber membrane group (PG), CuCS fiber membrane group (CuCS), Cur fiber membrane group (Cur), and CuCS + Cur fiber membrane group (CuCS/Cur). The mice were randomly assigned to the groups, with 6 mice in each group. A custom-made metal iron rod ($\Phi =$ 10 mm) was immersed in boiling water at 100 °C for over 10 min. It was then pressed onto the mouse's back for 5 s, resulting in deep third-degree burn wounds (average area 80 mm^2). Subsequently, the burn wounds were disinfected with 75 % alcohol for 10 s. Different fiber membranes (PG, CuCS, Cur, CuCS/Cur) were applied to the wounds and securely covered with 3 M wound dressing. Medical gauze served as the negative control group (Blank). The burned mice were monitored daily to observe wound healing progress.

2.10. Wound healing rate

Photographs of the wound area were captured on days 0, 1, 3, 6, and 12 post-surgery. The size of the wound area at various time points was assessed using Photoshop CS 6.0, and the wound healing rate was calculated based on the percentage of the healed area relative to the original burn wound area.

2.11. Histological analysis

Tissue samples were obtained on postoperative days 6 and 12 and subjected to fixation in 4 % paraformaldehyde for 48 h. Following paraffin embedding, the tissue samples were sectioned into 7 μm slices. For histological analysis, the sections were stained with hematoxylin and eosin (H&E, Sigma-Aldrich) according to the manufacturer's instructions. Immunostaining was performed by blocking the sections with 10 % goat serum in PBS for 1 h at room temperature. The primary antibody solution for cytokeratin 19 (sc-376126, Santa Cruz), rabbit anti-CD31 (ab9498, Abcam), or rabbit anti-neurocyte cytoplasmic protein 9.5 (SAB4503057, Sigma) was diluted in PBS to an appropriate ratio, and the samples were incubated at room temperature for 2 h. Subsequently, the sections were incubated with biotinylated goat anti-rabbit IgG (orb153693, Biorbit) as a secondary antibody, which was diluted in PBS, for 1 h at room temperature. The staining was visualized using DAB staining followed by hematoxylin staining. Tissue sections were examined under a microscope to analyze angiogenesis, collagen deposition, epithelialization, and hair follicle formation. The number of new hair follicles on day 12 was counted by selecting six random image areas from the cytokeratin 19 stained sections. The lengths of newborn nerves were counted on days 6 and 12 by selecting six random image areas from the PGP 9.5 stained sections. The number of new blood vessels on the 6th and 12th day was counted by selecting six random image areas from the CD31-stained sections.

2.12. Effects of Cu^{2+}-Cur chelate on the viability of HUVECs, HHDPCs and PC12

The previously prepared chelation solution of Cu^{2+} (6.25 μg/mL) and Cur (2 μg/mL) was taken, and fetal bovine serum, growth supplements, penicillin, and streptomycin were added in proportion. HUVECs (1×10^3/well), HHDPCs (1×10^3/well), or PC12 cells (1×10^3/well) were seeded in a 96-well culture plate. After 24 h of culture, the cell culture medium was replaced with the prepared chelating solution. Cu^{2+} ions alone and Cur alone were used as controls. On pre-set days 1, 3, and 5, the cell viability of all samples was assessed by measuring the absorbance using CCK-8 at 450 nm on a microplate reader.

2.13. Effects of Cu^{2+}-Cur chelate on the migration of HUVECs, HHDPCs and PC12

The previously prepared chelation solution of Cu^{2+} (6.25 μg/mL) and Cur (2 μg/mL) was taken, and fetal bovine serum, growth supplements, penicillin, and streptomycin were added in proportion. Cells were seeded in six-well plates (1×10^6/well) and cultured until reaching approximately 80 % confluency. Subsequently, the cells were starved for 24 h without serum to reset the cell cycle. The cell monolayer in each well was then scraped off with a plastic tip (200 μL), washed with PBS (0 h), and the cell culture medium was replaced with the prepared Cu^{2+}-Cur chelation solution. Cu^{2+} ions alone and Cur alone were used as controls. After incubation for 12 h in a 37 °C cell incubator, the cells

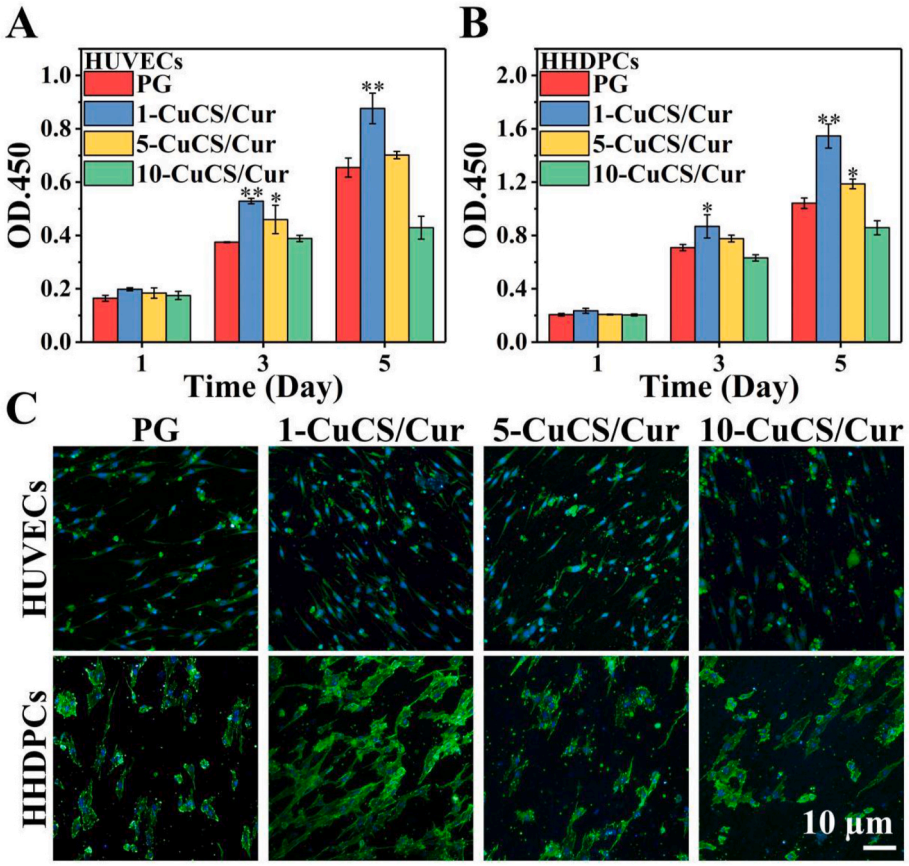

Fig. 2. Biological activity characterization of CuCS/Cur. (A, B) Effect of CuCS/Cur on the viability of HUVECs and HHDPCs. n = 6. (C) Representative immunofluorescence staining images of HUVECs and HHDPCs treated with CuCS/Cur. (*p < 0.05, **p < 0.01).

were stained with crystal violet (CV) for 1 min, and optical pictures were captured using light microscopy. The ratio of the initial scratch area to the final scratch area was subsequently analyzed using ImageJ software to determine the cell migration rate.

2.14. Effect of Cu^{2+}-Cur chelate on expression of neural-related factors in HHDPCs and PC12

Gene expression of GFAP and β-tubulin in HHDPCs, and PC12 cells was detected by quantitative PCR. Briefly, cells were seeded on 6-well culture plates at a density of 1×10^5 cells per well. The cells were then treated with the aforementioned media for 72 h. Subsequently, the cells were washed twice with preheated PBS, and total RNA was extracted from the cells using Trizol reagent (Invitrogen, USA). The concentration of total RNA was measured using a nanodrop 2000 reader (Thermo Scientific, USA). Following that, cDNA was synthesized using a Prime-Script™ RT reagent kit (Takara Bio, Shiga, Japan) according to the manufacturer's instructions. Primers for the stem cell markers, including GFAP and α-tubulin, as well as the housekeeping gene GAPDH, were commercially synthesized (Shengong, Co. Ltd. Shanghai, China). The quantification of all cDNA samples of stemness marker genes was performed using the Bio-Rad MyiQ single-color Real-time PCR system. All experiments were conducted in triplicate to obtain average data. The primer sequences were as follows: For human cells: GFAP: 5′-AAC CAA CCA CGC GAT TGT G-3′ and 5′-AAG TCT CAT CGT CCC ACC TC-3′; β-Tubulin: 5′-AAT TCC AAC TGC CAC TGT CC-3′ and 5′-GAC ATG GAT CCT GCC AAC TT-3′; GAPDH: 5′-CTG GGC TAC ACT GAG CAC C-3′ and 5′-AAG TGG TCG TTG AGG GCA ATG-3′. For rat cells: GFAP: 5′-GCA AGA AAC AGA AGA GTG GT-3′ and 5′-TTG GCG GCG ATA GTC ATT AG-3′; β-Tubulin: 5′-CCT TCA TCG GCA ACA GCA CG-3′ and 5′-GCC TCG GTG AAC TCC ATC TC-3′; GAPDH: 5′-TGC ACC ACC AAC TGC TTA G-3′ and 5′-GGA TGC AGG GAT GAT GTT C-3′.

2.15. Statistical analysis

All results were expressed as mean ± standard deviation. One-way ANOVA test was conducted to perform multiple comparisons between groups. Statistical significance was considered significant at $P < 0.05$ (*), $P < 0.01$ (**), or $P < 0.001$ (***).

3. Results

3.1. The characterization and cytocompatibility of the copper-doped calcium silicate ceramics/curcumin (CuCS/Cur) composite electrospun fiber membrane

Electrospun fiber membranes (polycaprolactone/gelatin) loaded with varying ratios of CuCS and curcumin (1-CuCS/Cur, 5-CuCS/Cur, and 10-CuCS/Cur) were prepared. From the optical photos, it was evident that as the concentration of CuCS and Cur increases, the color of the fiber membrane darkens (Fig. 1B). Additionally, we observed that loading ratios of 1 % and 5 % (1-CuCS/Cur and 5-CuCS/Cur) do not significantly impact the microscopic morphology of the fibers. However, at a loading amount of 10 % (10-CuCS/Cur), the presence of numerous irregular filaments suggested a reduction in the polymer's spinnability (Fig. 1C). Furthermore, we characterized the release behavior of the fiber membrane in terms of drug and ion release (Fig. 1D and E). It was observed that as the loading of CuCS and Cur increased, the release of Cu^{2+} and Cur also increased. Specifically, on day 5, the Cu^{2+} release from 1-CuCS/Cur, 5-CuCS/Cur, and 10-CuCS/Cur was measured at 21.06 ± 0.02 μg/mL, 36.08 ± 0.03 μg/mL, and 75.02 ± 0.08 μg/mL, respectively. The cumulative release of Cur on day 5 was 2.78 ± 0.04

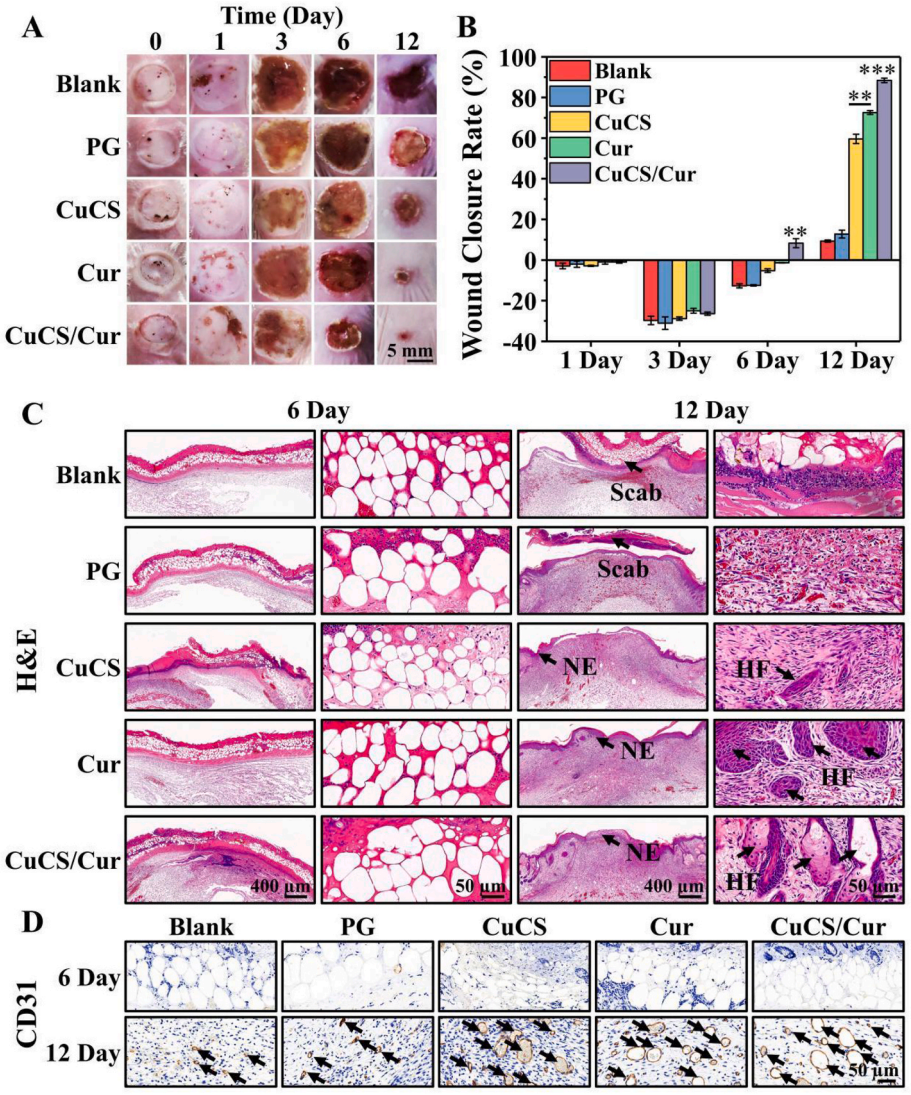

Fig. 3. Effect of CuCS/Cur on the treatment of third-degree skin burn wounds in mice. (A) Representative photographs depicting the burn wound area after different treatments. (B) Wound healing percentage following different treatments. n = 6. (C) Representative images of H&E staining showing burn wounds at days 6 and 12 (NE: new epidermis; HF: hair follicles). (D) Representative images of CD31 staining illustrating burn wounds at days 6 and 12 (Black arrows indicate new blood vessels). (**p < 0.01, ***p < 0.001).

μg/mL, 4.91 ± 0.05 μg/mL, and 9.24 ± 0.06 μg/mL, respectively.

Then, human umbilical vein endothelial cells (HUVECs) and human hair follicle dermal papilla cells (HHDPCs) were used to explore the cytocompatibility of fibrous membranes. CCK8 assay results demonstrated that both 1-CuCS/Cur and 5-CuCS/Cur significantly enhanced the cell viability of HUVECs and HHDPCs, with 1-CuCS/Cur exhibiting the most notable effect. However, 10-CuCS/Cur displayed evident cytotoxicity (Fig. 2A and B). Additionally, Phalloidin/DAPI staining revealed that the 1-CuCS/Cur fiber membrane exhibited the highest cell density in both HUVECs and HHDPCs (Fig. 2C).

3.2. The effect of CuCS/Cur on deep third degree burn model in mice

Based on the above findings, 1-CuCS/Cur was selected for animal experiments, and a control group was prepared consisting of an electrospun fiber membrane loaded with the same content of either CuCS or Cur (Blank: Medical gauze; PG: Pure electrospun fiber membrane prepared with polycaprolactone and gelatin; CuCS: Electrospun fiber membrane loaded with CuCS; Cur: Electrospun fiber membrane loaded with Cur; CuCS/Cur: Electrospun fiber membrane loaded with both CuCS and Cur).

As shown in Fig. 3A, within the first 3 days, the burn wound area of each group gradually expanded, and a substantial amount of scabs became apparent. On the 6th day, a significant decrease in wound area was observed following CuCS/Cur treatment. However, no notable difference was observed between the other groups and the Blank group. By the 12th day, the wounds in the Cur and CuCS/Cur groups were nearly completely healed, in comparison to the Blank group, the PG group, and the CuCS group. The healing trend of wounds was also supported by quantitative statistical results (Fig. 3B).

H&E staining was then employed to monitor the progression of skin healing (Fig. 3C). On the 6th day, the dermis of all groups exhibited numerous cavities resulting from burns, with no significant differences observed between the groups. By the 12th day, the dermis layers in the CuCS/Cur and Cur groups were completely healed, accompanied by a substantial generation of new hair follicle tissue. In contrast, the CuCS group displayed minimal hair follicle tissue formation. Additionally, while the dermis of the PG group had healed, a noticeable layer of scab remained on the wound surface. Conversely, the wounds in the Blank group not only displayed evident scabs but also exhibited incomplete healing in the dermis layer. Furthermore, we observed that the epithelial layer in both the CuCS/Cur group and the Cur group healed almost

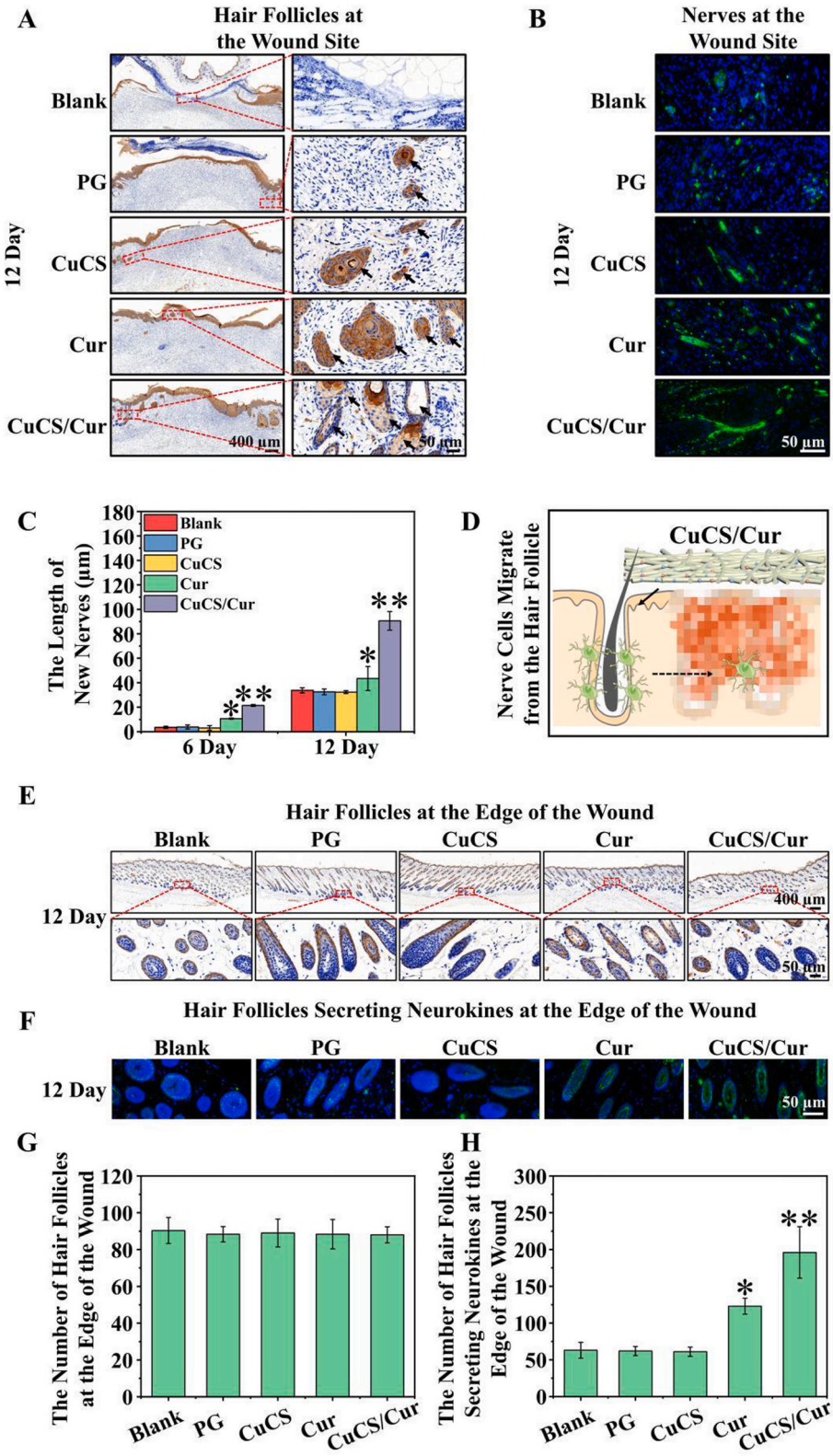

Fig. 4. Hair follicle and nerve regeneration induced by CuCS/Cur in the third-degree burn area. (A) Representative images of Cytokeratin 19 (K19) staining showing burn wounds at day 12 (Black arrows indicate new hair follicles). (B) Representative images of Protein Gene Product 9.5 (PGP 9.5) immunofluorescent staining showing new nerves at the burn wound site at day 12 (green fluorescence represents new nerves). (C) Quantification of the length of new nerves. n = 6. (D) CuCS/Cur induces the neural crest in the dermal papilla region of hair follicles to release precursor cells with neural differentiation potential, thereby promoting their differentiation into nerves and facilitating nerve regeneration. (E) Representative images of cytokeratin 19 (K19) staining showing newborn hair follicles at the edge of the burn wound at day 12. (F) Representative images of PGP 9.5 immunofluorescence staining illustrating hair follicles at the edge of the burn wound at day 12 (Green fluorescence indicates newborn nerve cells within the hair follicle). (G) Quantification of newborn hair follicles at the edge of the burn wound at day 12. n = 6. (H) Quantification of hair follicles secreting neurokines at the edge of the burn wound at day 12. n = 6. (*p < 0.05, **p < 0.01). (For interpretation of the references to color in this figure legend, the reader is referred to the Web version of this article.)

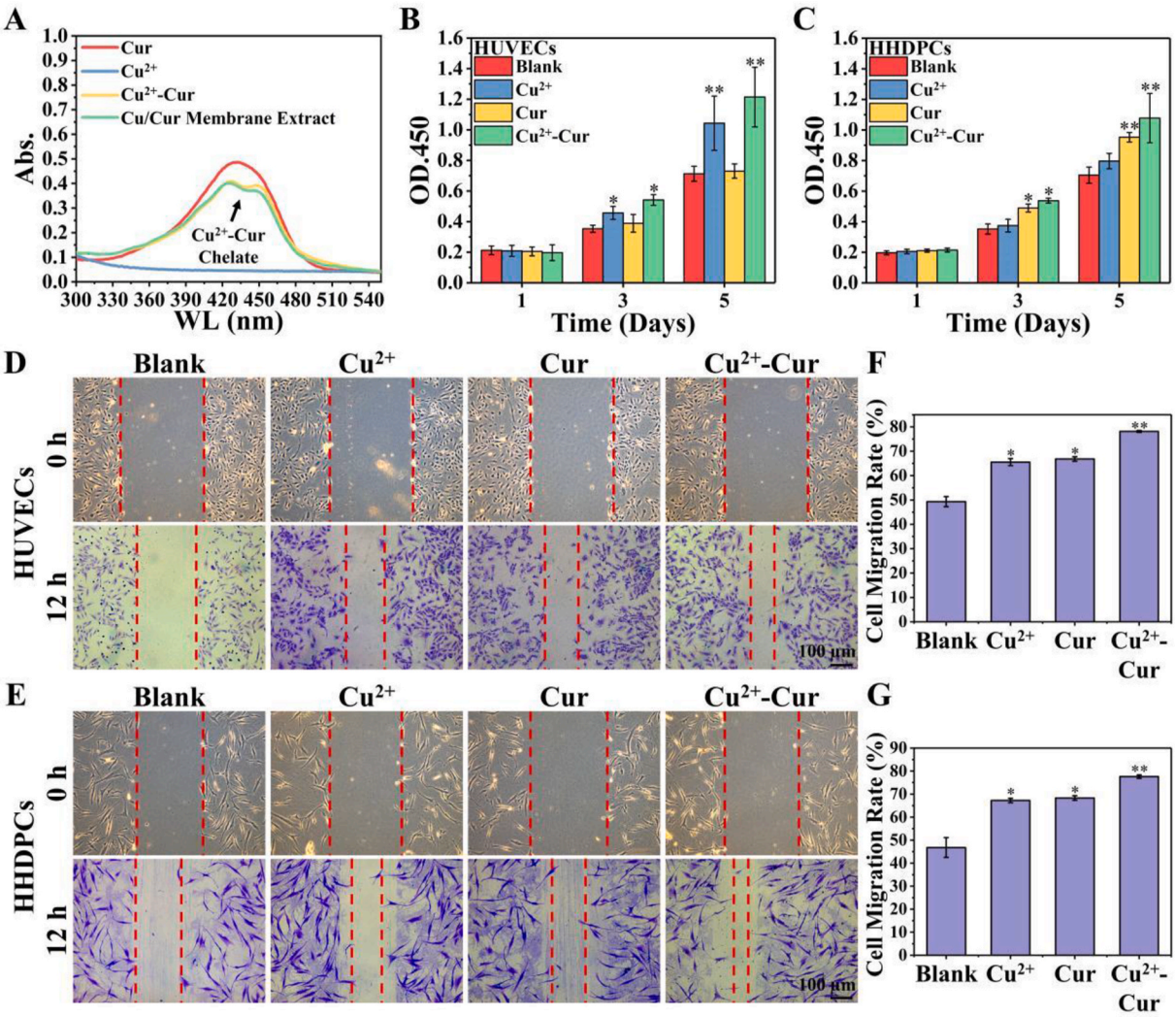

Fig. 5. Effect of Cu^{2+}-Cur chelate on HUVECs and HHDPCs. (A) UV absorption spectrum of CuCS/Cur electrospun fiber membrane extract (The control group consisted of a mixed solution of Cu^{2+} and Cur with varying concentrations). (B, C) Effect of Cu^{2+}-Cur chelate on the cell viability of HUVECs and HHDPCs (Cu^{2+} alone and Cur alone served as control groups, while DMEM was used as the Blank group). n = 6. (D, E) Effect of Cu^{2+}-Cur chelate on cell migration of HUVECs and HHDPCs (Cu2+ alone and Cur alone served as control groups, while DMEM was used as the Blank group). (F, G) Quantitative analysis of the cell migration rate of HUVECs and HHDPCs. n = 6. (*p < 0.05, **p < 0.01).

completely on the 12th day. The H&E staining images shows that the dark pink epithelial layer has formed tight connections. In contrast, despite the emergence of new epithelial layers, they had not formed continuous connection in the CuCS groups, while in PG and Blank groups the epithelial layers were entirely obstructed by scar tissue (Fig. 3C).

To observe angiogenesis at the wound site, CD31 staining was utilized (Fig. 3D). Although no notable CD31-positive staining was observed in the wound area of any group on the 6th day, a remarkable discovery was made on the 12th day. Comparatively, the CuCS, Cur, and CuCS/Cur groups exhibited a significant production of new blood vessels, surpassing both the Blank group and the PG group. However, the quantitative statistical analysis showed no significant differences among these three groups (Fig. S1).

3.3. CuCS/Cur promotes hair follicle and nerve regeneration in the third-degree burn wound area

Cytokeratin 19 (K19) immunohistochemical staining was initially employed to observe hair follicle regeneration at the wound site (Fig. 4A and Fig. S2). On day 6, no new hair follicle precursors were observed in the wound area of any group. However, by day 12, a distinct phenomenon occurred as a significant accumulation of hair follicle cells commenced, resulting in the formation of hair follicle precursors in the PG group, CuCS group, Cur group, and CuCS/Cur group. Remarkably, in the CuCS/Cur group, the hair follicle precursors had already initiated the process of differentiating into mature hair follicle tissue. Quantitative analysis further substantiated that CuCS/Cur significantly enhanced hair follicle regeneration at the wound site compared with the CuCS and Cur groups (Fig. S3). Furthermore, Protein Gene Product 9.5 (PGP 9.5) immunofluorescence staining was utilized to investigate nerve regeneration within the wound area (Fig. 4B and Fig. S4). On the 6th day, only a minimal amount of PGP 9.5 positive staining was detected in the Cur and CuCS/Cur groups. In contrast, there was an almost negligible presence of PGP 9.5 positive staining in the Blank, PG, and CuCS groups. By the 12th day, positive PGP 9.5 staining was observed in the wound area of all groups, indicating the initiation of nerve tissue regeneration. Notably, in the CuCS/Cur group, the neural tissue started extending into elongated strands resembling neural networks. Quantitative statistical analysis confirmed that the length of nerve tissue in the CuCS/Cur group was the greatest, significantly surpassing that of the other groups (Fig. 4C).

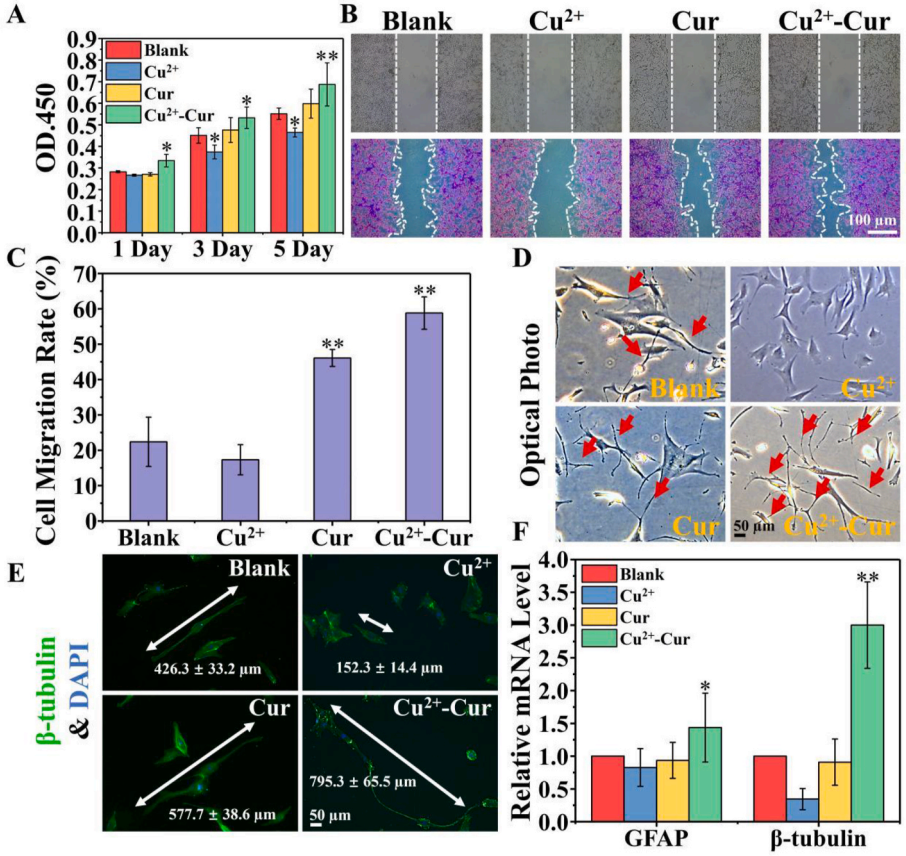

Fig. 6. Effect of Cu^{2+}-Cur chelate on the PC12 cells. (A) Effect of Cu^{2+}-Cur chelate on the cell viability of PC12 (Cu^{2+} alone and Cur alone served as control groups, while DMEM was used as the Blank group). n = 6. (B) Effect of Cu^{2+}-Cur chelate on cell migration of PC12 (Cu^{2+} alone and Cur alone served as control groups, while DMEM was used as the Blank group). (C) Quantitative analysis of the cell migration rate of PC12. n = 6. (D) Representative optical images of PC12 after Cu^{2+}-Cur chelate treatment (Cu^{2+} alone and Cur alone served as control groups, while DMEM was used as the Blank group). (E) Representative immunofluorescent staining of β-tubulin images of PC12 after Cu^{2+}-Cur chelate treatment (Cu^{2+} alone and Cur alone served as control groups, while DMEM was used as the Blank group). (F) PCR analysis of the expression of nerve-related proteins in Cu^{2+}-Cur chelate-treated PC12 cells (Cu^{2+} alone and Cur alone served as control groups, while DMEM was used as the Blank group). n = 6. (*$p < 0.05$, **$p < 0.01$).

3.4. CuCS/Cur enhances the supply of nerve-related cells from hair follicles to promote nerve regeneration

Given that hair follicles are the main source of cutaneous nerve-related cells, we speculated that CuCS/Cur might have the ability to activate hair follicle tissue around burn wounds, thereby promoting nerve regeneration in the damaged area (Fig. 4D). Therefore, we first observed hair follicle growth at the wound edge. Specifically, by day 12, a large amount of fully mature hair follicle tissue had formed at the wound edge in all groups (Fig. 4E). Interestingly, some hair follicles indeed highly expressed PGP 9.5, indicating that they were secreting nerve-related cells. Particularly in the CuCS/Cur group, PGP 9.5 was highly expressed in almost all hair follicles (Fig. 4F). Through further quantitative analysis, we found that there was almost no significant difference in the number of new hair follicles around the burn wound in each group (Fig. 4G). However, after treatment with CuCS/Cur and Cur, a large number of new hair follicles expressing PGP 9.5 were produced, with the CuCS/Cur group showing the highest expression levels (Fig. 4H).

3.5. The effect of Cu^{2+}-Cur chelate on skin-related cells

When inorganic ions and flavonoids are present together, they have the ability to form highly bioactive chelates [6–8]. These chelates may play a crucial role in promoting wound healing when using CuCS/Cur wound dressing. To investigate this, the release of Cu^{2+}-Cur chelate from CuCS/Cur was examined firstly using a UV spectrophotometer, with mixed solutions of Cur and Cu^{2+} at different ratios used as control samples. Interestingly, as Cu^{2+} was gradually added to the Cur solution, the characteristic absorption peak of Cur at 425 nm started to decrease and split into two distinct absorption peaks. This phenomenon indicated the formation of Cu^{2+}-Cur chelate. Similarly, the extract obtained from the CuCS/Cur fiber membrane also exhibited the same characteristic absorption peak at 425 nm. This finding confirms that the composite fiber membrane is capable of releasing the Cu^{2+}-Cur chelate (Fig. 5A).

To further investigate the effects of the Cu^{2+}-Cur chelate on skin-related cells, the cell viability of HUVECs and HHDPCs was assessed using the CCK8 assay (Fig. 5B and C). It was observed that the Cu^{2+}-Cur chelate significantly enhanced the viability of both cell types within 5 days. In contrast, Cu^{2+} alone only slightly increased the cell viability of HUVECs, and Cur alone only slightly increased the cell viability of HHDPCs. Moreover, the Cu^{2+}-Cur chelate exhibited the greatest ability to promote cell migration in both HUVECs and HHDPCs (Fig. 5D and E). Quantitative statistical analysis displayed that after stimulation with the Cu^{2+}-Cur chelate for 12 h, the cell migration rate of HUVECs reached 78.11 ± 0.39 % (Fig. 5F), while that of HHDPCs reached 77.60 ± 0.74 % (Fig. 5G). These values were 1.15–1.19 times higher than those achieved with Cu^{2+} alone and 1.13–1.17 times higher than those achieved with Cur alone. Although Cu^{2+} alone and Cur alone also exhibited a slight promotion of cell migration ability in HUVECs and HHDPCs.

3.6. The effects of Cu^{2+}-Cur chelate on the secretion of neural-related factors in HHDPCs

The effect of the Cu^{2+}-Cur chelate on the expression of nerve-related factors in HHDPCs is also crucial in determining its effect on nerve regeneration during the process of wound repair. Therefore, the expressions of glial fibrillary acidic protein (GFAP) and β-tubulin in HHDPCs treated with the Cu^{2+}-Cur chelate were assessed using PCR (Fig. S5). The findings revealed that the Cu^{2+}-Cur chelate significantly enhanced the expression of GFAP and β-tubulin in HHDPCs. In contrast, Cur alone exhibited a slight promotion of GFAP and β-tubulin expression in HHDPCs, while Cu^{2+} alone did not show any notable enhancement. These results indicate that the Cu^{2+}-Cur chelate indirectly promotes nerve regeneration by stimulating the secretion of nerve-associated GFAP and β-tubulin through HHDPCs.

3.7. The effects of Cu^{2+}-Cur chelate on neural-related rat adrenal medulla pheochromoma differentiated cell line (PC12)

The Cu^{2+}-Cur chelate was utilized to treat the neural-related rat adrenal medulla pheochromoma differentiated cell line (PC12) in order to assess its direct potential in promoting nerve regeneration. The results of the CCK8 assay demonstrated that the Cu^{2+}-Cur chelate significantly enhanced the cell viability of PC12 cells on the 1st day, with further improvements observed on the 3rd and 5th day (Fig. 6A). Notably, on the 5th day, the cell viability of PC12 cells treated with the Cu^{2+}-Cur chelate was 1.25 times higher than that of the Blank group. In contrast, Cur alone exhibited no effect on the viability of PC12 cells, while Cu^{2+} alone displayed an inhibitory effect on PC12 cells on the 3rd and 5th day. Moreover, the Cu^{2+}-Cur chelate was found to significantly enhance the cell migration ability of PC12 cells (Fig. 6B). Quantitative statistical analysis further revealed that the cell migration rate of PC12 cells treated with the Cu^{2+}-Cur chelate was 2.63 times higher than that of the Blank group (Fig. 6C). Comparatively, the cell migration rate of PC12 cells treated with Cur alone was 2.06 times higher than that of the Blank group. Additionally, Cu^{2+} alone exhibited an inhibitory effect on the migration of PC12 cells.

Light microscopy (Fig. 6D) and immunofluorescence staining of β-tubulin (Fig. 6E) were employed to examine PC12 cells treated with Cu^{2+}-Cur chelate. The results revealed that the Cu^{2+}-Cur chelate significantly promoted neurite growth in PC12 cells, while the effect of Cur alone was not apparent. Conversely, Cu^{2+} alone exhibited a notable inhibitory effect. PCR data further demonstrated that only the Cu^{2+}-Cur chelate significantly increased the expression of GFAP and β-tubulin in PC12 cells, whereas Cu^{2+} alone significantly suppressed the expression of β-tubulin (Fig. 6F).

4. Discussion

While numerous studies have developed a range of wound dressings that have achieved remarkable results in skin regeneration [36], most wound dressings primarily focus on wound closure by promoting fibroblast proliferation and do not address the reconstruction of the neural network beneath the dermis. As a result, many patients with deep burns often report loss of cutaneous sensation after wound healing [41]. Consequently, restoring skin pain, temperature, and touch perception has become a significant challenge to enhance patients' quality of life. To address this problem, researchers have proposed various treatment methods, including activating nerve cells through electrical stimulation, or using drugs to inhibit the activity of fibroblasts around nerve endings, thereby facilitating nerve regeneration within the wound site [42,43]. However, these treatment strategies paradoxically do not have a positive effect on wound healing itself and may even inhibit the rate of wound closure, increase the risk of infection and malignant transformation, and potentially result in life-threatening risks in severe cases [44]. In contrast, in this study, we developed an electrospun wound dressing composed of copper-doped calcium silicate and curcumin (CuCS/Cur), a composite fibrous membrane capable of efficiently releasing bioactive Cu^{2+} and SiO_3^{2-} ions and Cur to significantly promote nerve regeneration with rapid skin healing.

The prerequisite for reconstructing the skin neural network is to have an ample supply of nerve cells. The introduction of exogenous stem cells with neural differentiation potential is perhaps the most common strategy employed to replenish subcutaneous neurons. For instance, Tomita et al. discovered that adipose-derived stem cells exhibited a robust neurite response in vitro and effectively treated acute and chronic sciatic nerve denervation injuries in rats [45,46]. Amoh et al. implanted hair follicle stem cells near severed peripheral nerves and observed that these cells rapidly differentiated into Schwann cells, promoting peripheral nerve repair [47]. However, to date, no studies have explored the injection of stem cells into burned areas to induce nerve regeneration. This may be due to the fact that these exogenous cells have a greater propensity to differentiate into other skin repair-related cells rather than neurocytes since the wound microenvironment is complicated [20,48,49]. Additionally, even these exogenous cells manage to differentiate into hair follicle tissue, the production of nerve cells by normal hair follicles is relatively limited due to the low differentiation rate [14,50]. In contrast to these cell therapies, the major advantage of the CuCS/Cur composite dressing designed in this study is its ability to stimulate regeneration of the hair follicle tissue, which functions as a nerve cell generating "factory" [16] in the wound area, and promotes nerve cell production and nerve regeneration (Fig. 4B and F). Upon carefully dissecting the main reason for the unique effect of CuCS/Cur, we discovered that the Cu^{2+}-Cur chelate released from the composite wound dressing serves as the core bioactive component for rebuilding and re-energizing the "factory". Our previous studies have proved that the chelation synergistic effect of active ions (Cu^{2+}, Zn^{2+}) released from silicate bioceramics and flavonoids (Quercetin) can greatly enhance hair follicle regeneration in burn wounds [6–8,51]. Here, we futher demonstrated that the Cu^{2+}-Cur chelate not only significantly enhances the proliferation and migration abilities of hair follicle dermal papilla cells but also greatly increases the expression of nerve-related factors, such as GFAP and β-tubulin (Fig. S5). Building upon this foundation, the present study further confirms that this chelation synergistic effect also has a positive impact on the functionality of hair follicles, including the production of nerve cells. It is worth to indicate that although we used Cur in this study, other flavonoids with similar bioactivity such as quercetin and apigenin may also be able to form chelates with Cu^{2+} ions, and exhibit nerve regeneration-promoting activity [52]. Therefore, it is worth to consider further studies to compare the bioactivities of other flavonoids-Cu chelates in stimulating hair follicles and neuralized skin regeneration.

Rapid skin healing plays a significant role in enhancing skin nerve regeneration by providing a more favorable growth environment for nerves. This is because a more intact blood vessel network within the healed skin can provide more nutrients for nerve growth [53]. Additionally, rapid healing is accompanied with earlier maturation of hair follicle tissue, which further supports nerve regeneration [14,15]. It is worth mentioning that previous studies have demonstrated the significant impact of SiO_3^{2-} ions released from silicate bioceramics in accelerating skin wound healing [54,55]. Therefore, it is reasonable to speculate that SiO_3^{2-} released by CuCS/Cur also positively contributes to skin nerve regeneration by stimulating wound healing rate. However, despite the significant promotion of blood vessel and hair follicle regeneration at the wound site by CuCS used in this study, it did not notably enhance nerve regeneration. We postulate that this could be attributed to the release of Cu^{2+} from CuCS, which may inhibit nerve regeneration, given that Cu^{2+} is known to be neurotoxic when present alone [56,57]. Therefore, while CuCS/Cur aids in increasing the presence of neural precursor cells in the burn wound area, it is important to consider whether the presence of Cu^{2+} will impede the further neural differentiation. Interestingly, our study revealed that although Cu^{2+}

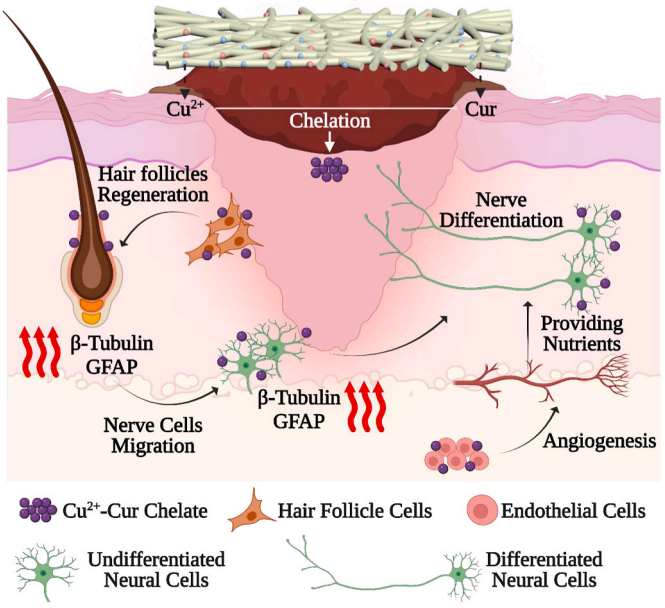

Fig. 7. A composite electrospun fibrous membrane (CuCS/Cur) consisting of copper-doped calcium silicate ceramic (CuCS) and curcumin (Cur) was developed and designed for the regeneration of neuralized skin following deep skin burns. This composite fiber membrane has the ability to efficiently release biologically active Cu^{2+} ions and Cur. The chelation effect of these two released products forms a highly bioactive Cu^{2+}-Cur chelate, which is primarily responsible for the following key aspects of neural regeneration. Firstly, the Cu^{2+}-Cur chelate activates hair follicle cells, leading to accelerated hair follicle regeneration, and then significantly enhances the expression of nerve-related factors, such as β-Tubulin and GFAP, within the hair follicles. This activation stimulates the neural crest in the dermal papilla area to secrete precursor cells with neural differentiation potential. Moreover, the Cu^{2+}-Cur chelate directly stimulates neural differentiation of these undifferentiated neurons. Additionally, it promotes the differentiation of endothelial cells into vascular tissue, ensuring an adequate supply of nutrients to the nerve cells. This indirect effect further promotes nerve regeneration.

alone significantly inhibited various cellular activities of PC12 cells, the chelation effect between Cu^{2+} and Cur not only reduced the toxicity of Cu^{2+} to nerve cells [56,57] but also elevated the neurorestorative efficacy of Cur to a new level [58–60]. Studies have shown that when Cu^{2+} forms a chelate with certain polypeptides in the human body, it can effectively stimulate the secretion of nerve growth factors in skin-related cells and promote nerve regeneration [61,62]. Similarly, flavonoids such as Cur may function like human polypeptides and bind to excess Cu^{2+}. This not only alleviates the neurotoxicity of the excess Cu^{2+} but also retains its functions in promoting angiogenesis, which is beneficial for the regeneration of either hair follicles or the reconstruction of the cutaneous nervous system.

5. Conclusion

In this study, a wound dressing called CuCS/Cur was designed, which incorporated copper-doped calcium silicate (CuCS) and curcumin (Cur). This innovative dressing demonstrated significant efficacy in promoting nerve regeneration in deep third-degree skin wounds. The key to its unique biological activity lied in the Cu^{2+}-Cur chelate released by CuCS/Cur. This chelate primarily rebuilt the "factory" responsible for producing nerve cells by inducing hair follicle regeneration. Simultaneously, it greatly enhanced the expression of nerve-related factors within the hair follicle, injecting energy into the "factory" and accelerating the production of nerve cells. Notably, the Cu^{2+}-Cur chelate itself possessed an excellent ability to induce neural differentiation, thereby promoting the transformation of nerve cells generated by hair follicles into a fully functional neural network. Moreover, the Cu^{2+}-Cur chelate also exhibited a remarkable capacity to promote capillary regeneration, providing ample nutrients for skin wound healing, hair follicle regeneration, and nerve regeneration (Fig. 7). This study confirmed that the chelation synergistic effect between bioactive ions and flavonoids enables systemic regulation of the entire population of skin-related cells, establishing a solid foundation for the development of wound dressings capable of achieving perfect skin tissue regeneration.

CRediT authorship contribution statement

Zhaowenbin Zhang: Writing – review & editing, Writing – original draft, Project administration, Data curation. **Di Chang:** Writing – original draft, Investigation, Formal analysis. **Zhen Zeng:** Writing – original draft, Investigation. **Yuze Xu:** Project administration. **Jing Yu:** Investigation. **Chen Fan:** Formal analysis. **Chen Yang:** Writing – review & editing, Writing – original draft, Investigation, Formal analysis. **Jiang Chang:** Writing – review & editing, Writing – original draft, Resources, Investigation, Funding acquisition.

Declaration of competing interest

The author(s) declared no potential conflicts of interest with respect to the research, author-ship, and/or publication of this article.

Data availability

Data will be made available on request.

Acknowledgements

This research was supported by the China Postdoctoral Science Foundation (GZB20230736, 2023M733463, 2023M743444), the National Natural Science Foundation of China (No. 32301096, 32101067), the Wenzhou Science and Technology Major Project (ZY2022028), the Wenzhou Science and Technology Project (Y20220142), the Open Project of the Key Laboratory of Rehabilitation Medicine in Sichuan Province (KFYXSZDSYS-01), the Natural Science Foundation of Sichuan Province, China (2022NSFSC1469), the seed grants from the Wenzhou Institute, University of Chinese Academy of Sciences (WIUCASQD2020013, WIUCASQD2021029, WIUCASQD2021030), and the founding from the First Affiliated Hospital of Wenzhou Medical University.

Appendix A. Supplementary data

Supplementary data to this article can be found online at https://doi.org/10.1016/j.mtbio.2024.101075.

References

[1] M. Blais, R. Parenteau-Bareil, S. Cadau, F. Berthod, Concise review: tissue-engineered skin and nerve regeneration in burn treatment, Stem Cells Translational Medicine 2 (7) (2013) 545–551.
[2] Y. Hu, B. Yu, Y. Jia, M. Lei, Z. Li, H. Liu, H. Huang, F. Xu, J. Li, Z. Wei, Hyaluronate- and gelatin-based hydrogels encapsulating doxycycline as a wound dressing for burn injury therapy, Acta Biomater. 164 (2023) 151–158.
[3] X. Shi, T. Zhou, S. Huang, Y. Yao, P. Xu, S. Hu, C. Tu, W. Yin, C. Gao, J. Ye, An electrospun scaffold functionalized with a ROS-scavenging hydrogel stimulates ocular wound healing, Acta Biomater. 158 (2023) 266–280.
[4] Y. Feng, L. Su, Z. Zhang, Y. Chen, M.R. Younis, D. Chen, J. Xu, C. Dong, Y. Que, C. Fan, pH-responsive wound dressing based on biodegradable CuP nanozymes for treating infected and diabetic wounds, ACS Appl. Mater. Interfaces 16 (1) (2023) 95–110.
[5] J.F. Xu, M.R. Younis, Z.W.B. Zhang, Y.P. Feng, L.F. Su, Y.M. Que, Y.R. Jiao, C. Fan, J. Chang, S.Y. Ni, C. Yang, Mild heat-assisted polydopamine/alginate hydrogel containing low-dose nanoselenium for facilitating infected wound healing, ACS Appl. Mater. Interfaces 15 (6) (2023) 7841–7854.
[6] Z.W.B. Zhang, Q.X. Dai, Y. Zhang, H. Zhuang, E.D. Wang, Q. Xu, L.L. Ma, C.T. Wu, Z.G. Huan, F. Guo, J. Chang, Design of a multifunctional biomaterial inspired by

ancient Chinese medicine for hair regeneration in burned skin, ACS Appl. Mater. Interfaces 12 (11) (2020) 12489–12499.
[7] Z.W.B. Zhang, W.B. Li, Y. Liu, Z.G. Yang, L.L. Ma, H. Zhuang, E.D. Wang, C.T. Wu, Z.G. Huan, F. Guo, J. Chang, Design of a biofluid-absorbing bioactive sandwich-structured Zn-Si bioceramic composite wound dressing for hair follicle regeneration and skin burn wound healing, Bioact. Mater. 6 (7) (2021) 1910–1920.
[8] Z.W.B. Zhang, Y. Zhang, W.B. Li, L.L. Ma, E.D. Wang, M. Xing, Y.L. Zhou, Z. G. Huan, F. Guo, J. Chang, Curcumin/Fe-SiO_2 nano composites with multi-synergistic effects for scar inhibition and hair follicle regeneration during burn wound healing, Appl. Mater. Today 23 (2021) 101065.
[9] S.C. Kellaway, V. Roberton, J.N. Jones, R. Loczenski, J.B. Phillips, L.J. White, Engineered neural tissue made using hydrogels derived from decellularised tissues for the regeneration of peripheral nerves, Acta Biomater. 157 (2023) 124–136.
[10] W. Xu, Y. Wu, H. Lu, X. Zhang, Y. Zhu, S. Liu, Z. Zhang, J. Ye, W. Yang, Injectable hydrogel encapsulated with VEGF-mimetic peptide-loaded nanoliposomes promotes peripheral nerve repair in vivo, Acta Biomater. 160 (2023) 225–238.
[11] M. Yang, B. Su, Z. Ma, X. Zheng, Y. Liu, Y. Li, J. Ren, L. Lu, B. Yang, X. Yu, Renal-friendly Li plus -doped carbonized polymer dots activate Schwann cell autophagy for promoting peripheral nerve regeneration, Acta Biomater. 159 (2023) 353–366.
[12] D. Kang, Z. Liu, C. Qian, J. Huang, Y. Zhou, X. Mao, Q. Qu, B. Liu, J. Wang, Z. Hu, Y. Miao, 3D bioprinting of a gelatin-alginate hydrogel for tissue-engineered hair follicle regeneration, Acta Biomater. 165 (2023) 19–30.
[13] Z. Liu, J. Huang, D. Kang, Y. Zhou, L. Du, Q. Qu, J. Wang, L. Wen, D. Fu, Z. Hu, Y. Miao, Microenvironmental reprogramming of human dermal papilla cells for hair follicle tissue engineering, Acta Biomater. 165 (2023) 31–49.
[14] Y. Amoh, L. Li, R. Campillo, K. Kawahara, K. Katsuoka, S. Penman, R.M. Hoffman, Implanted hair follicle stem cells form Schwann cells that support repair of severed peripheral nerves, Proc. Natl. Acad. Sci. USA 102 (49) (2005) 17734–17738.
[15] S. Ji, Z. Zhu, X. Sun, X. Fu, Functional hair follicle regeneration: an updated review, Signal Transduct. Targeted Ther. 6 (1) (2021) 66.
[16] M. Bhoopalam, L.A. Garza, S.K. Reddy, Wound induced hair neogenesis–a novel paradigm for studying regeneration and aging, Front. Cell Dev. Biol. 8 (2020) 582346.
[17] J. Zhang, R. Chen, L. Wen, Z. Fan, Y. Guo, Z. Hu, Y. Miao, Recent progress in the understanding of the effect of sympathetic nerves on hair follicle growth, Front. Cell Dev. Biol. 9 (2021) 736738.
[18] Y. Mukouyama, D. Shin, S. Britsch, M. Taniguchi, D.J. Anderson, Sensory nerves determine the pattern of arterial differentiation and blood vessel branching in the skin, Cell 109 (6) (2002) 693–705.
[19] C. Zhang, Y. Chen, X. Fu, Sweat gland regeneration after burn injury: is stem cell therapy a new hope? Cytotherapy 17 (5) (2015) 526–535.
[20] H. Li, M. Ziemer, I. Stojanovic, T. Saksida, D. Maksimovic-Ivanic, S. Mijatovic, G. Djmura, D. Gajic, I. Koprivica, T. Krajnovic, Mesenchymal stem cells from mouse hair follicles reduce hypertrophic scarring in a murine wound healing model, Stem Cell Rev. Rep. 18 (6) (2022) 2028–2044.
[21] R.S. Arzi, M. Davidovich-Pinhas, N. Cohen, A. Sosnik, An experimental and theoretical approach to understand the interaction between particles and mucosal tissues, Acta Biomater. 158 (2023) 449–462.
[22] J. Hou, Y. Cong, J. Ji, Y. Liu, H. Hong, X. Han, Spatial targeting of fibrosis-promoting macrophages with nanoscale metal-organic frameworks for idiopathic pulmonary fibrosis therapy, Acta Biomater. 174 (2024) 372–385.
[23] S. Sanchez-Salcedo, C. Heras, D. Lozano, M. Vallet-Regi, A.J. Salinas, Nanodevices based on mesoporous glass nanoparticles enhanced with zinc and curcumin to fight infection and regenerate bone, Acta Biomater. 166 (2023) 655–669.
[24] Y. Shen, Y. Zou, B. Bie, C. Dong, Y. Lv, Combining dual-targeted liquid metal nanoparticles with autophagy activation and mild photothermal therapy to treat metastatic breast cancer and inhibit bone destruction, Acta Biomater. 157 (2023) 578–592.
[25] E. Wang, A.V. Patel, S. Harel, Z. Dai, A.M. Christiano, Topical curcumin promotes induction of the murine hair cycle, J. Invest. Dermatol. 136 (5) (2016). S122-S122.
[26] C. Schiborr, A. Kocher, D. Behnam, J. Jandasek, S. Toelstede, J. Frank, The oral bioavailability of curcumin from micronized powder and liquid micelles is significantly increased in healthy humans and differs between sexes, Mol. Nutr. Food Res. 58 (3) (2014) 516–527.
[27] K.I. Priyadarsini, The chemistry of curcumin: from extraction to therapeutic agent, Molecules 19 (12) (2014) 20091–20112.
[28] Z. Gao, X. Yang, K. Huang, H. Xu, Free-radical scavenging and mechanism study of flavonoids extracted from the radix of Scutellaria baicalensis Georgi, Appl. Magn. Reson. 19 (1) (2000) 35–44.
[29] Z. Jurasekova, C. Domingo, J.V. Garcia-Ramos, S. Sanchez-Cortes, Effect of pH on the chemical modification of quercetin and structurally related flavonoids characterized by optical (UV-visible and Raman) spectroscopy, Phys. Chem. Chem. Phys. 16 (25) (2014) 12802–12811.
[30] R.W. Byard, Caustic ingestion-A forensic overview, J. Forensic Sci. 60 (3) (2015) 812–815.
[31] S. Hu, C.Q. Ning, Y. Zhou, L. Chen, K.L. Lin, J. Chang, Antibacterial activity of silicate bioceramics, J. Wuhan Univ. Technol.-Materials Sci. Ed. 26 (2) (2011) 227–231.
[32] S.L. Percival, S. McCarty, J.A. Hunt, E.J. Woods, The effects of pH on wound healing, biofilms, and antimicrobial efficacy, Wound Repair Regen. 22 (2) (2014) 174–186.
[33] X.T. Wang, L.Y. Wang, Q. Wu, F. Bao, H.T. Yang, X.Z. Qiu, J. Chang, Chitosan/calcium silicate cardiac patch stimulates cardiomyocyte activity and myocardial performance after infarction by synergistic effect of bioactive ions and aligned nanostructure, ACS Appl. Mater. Interfaces 11 (1) (2019) 1449–1468.
[34] P. Srinath, P.A. Azeem, K.V. Reddy, Review on calcium silicate-based bioceramics in bone tissue engineering, Int. J. Appl. Ceram. Technol. 17 (5) (2020) 2450–2464.
[35] Q. Yu, Y. Han, X. Wang, C. Qin, D. Zhai, Z. Yi, J. Chang, Y. Xiao, C. Wu, Copper silicate hollow microspheres-incorporated scaffolds for chemo-photothermal therapy of melanoma and tissue healing, ACS Nano 12 (3) (2018) 2695–2707.
[36] C. Fan, Q. Xu, R. Hao, C. Wang, Y. Que, Y. Chen, C. Yang, J. Chang, Multi-functional wound dressings based on silicate bioactive materials, Biomaterials 287 (2022) 121652.
[37] E.R. Ghomi, R. Lakshminarayanan, V. Chellappan, N.K. Verma, A. Chinnappan, R. E. Neisiany, K. Amuthavalli, Z.S. Poh, B.H.S. Wong, N. Dubey, R. Narayan, S. Ramakrishna, Electrospun aligned PCL/gelatin scaffolds mimicking the skin ECM for effective antimicrobial wound dressings, Advanced Fiber Materials 5 (1) (2022) 235–251.
[38] K. Ren, Y. Wang, T. Sun, W. Yue, H. Zhang, Electrospun PCL/gelatin composite nanofiber structures for effective guided bone regeneration membranes, Mater. Sci. Eng. C 78 (2017) 324–332.
[39] X. Guo, X. Wang, H. Tang, Y. Ren, D. Li, B. Yi, Y. Zhang, Engineering a mechanoactive fibrous substrate with enhanced efficiency in regulating stem cell tenodifferentiation, ACS Appl. Mater. Interfaces 14 (20) (2022) 23219–23231.
[40] B. Yi, L. Yu, H. Tang, W. Wang, W. Liu, Y. Zhang, Lysine-doped polydopamine coating enhances antithrombogenicity and endothelialization of an electrospun aligned fibrous vascular graft, Appl. Mater. Today 25 (2021) 101198.
[41] T.T. Weng, P. Wu, W. Zhang, Y.R. Zheng, Q. Li, R.H. Jin, H.J. Chen, C.G. You, S. X. Guo, C.M. Han, X.G. Wang, Regeneration of skin appendages and nerves: current status and further challenges, J. Transl. Med. 18 (1) (2020) 1–17.
[42] E.C. Soller, D.S. Tzeranis, K. Miu, P.T. So, I.V. Yannas, Common features of optimal collagen scaffolds that disrupt wound contraction and enhance regeneration both in peripheral nerves and in skin, Biomaterials 33 (19) (2012) 4783–4791.
[43] X.L. Chu, X.Z. Song, Q. Li, Y.R. Li, F. He, X.S. Gu, D. Ming, Basic mechanisms of peripheral nerve injury and treatment via electrical stimulation, Neural Regeneration Research 17 (10) (2022) 2185–2193.
[44] X. Fu, Wound healing center establishment and new technology application in improving the wound healing quality in China, Burns & Trauma 8 (2020) tkaa038.
[45] C.A. Kubiak, J. Grochmal, T.A. Kung, P.S. Cederna, R. Midha, S.W.P. Kemp, Stem-cell-based therapies to enhance peripheral nerve regeneration, Muscle Nerve 61 (4) (2020) 449–459.
[46] K. Tomita, T. Madura, C. Mantovani, G. Terenghi, Differentiated adipose-derived stem cells promote myelination and enhance functional recovery in a rat model of chronic denervation, J. Neurosci. Res. 90 (7) (2012) 1392–1402.
[47] Y. Amoh, L.N. Li, R. Campillo, K. Kawahara, K. Katsuoka, S. Penman, R. M. Hoffman, Implanted hair follicle stem cells form Schwann cells that support repair of severed peripheral nerves, Proc. Natl. Acad. Sci. U.S.A. 102 (49) (2005) 17734–17738.
[48] F. Liu, H.T. Zhou, W.B. Du, X.L. Huang, X. Zheng, C. Zhang, H.H. Hu, J.F. Wang, R. F. Quan, Hair follicle stem cells combined with human allogeneic acellular amniotic membrane for repair of full thickness skin defects in nude mice, J. Tissue Eng. Regen. Med. 14 (5) (2020) 723–735.
[49] S. Aslam, I. Khan, F. Jameel, M.B. Zaidi, A. Salim, Umbilical cord-derived mesenchymal stem cells preconditioned with isorhamnetin: potential therapy for burn wounds, World J, Stem Cell. 12 (12) (2020) 1652–1666.
[50] C.A. Jahoda, A.J. Reynolds, Hair follicle dermal sheath cells: unsung participants in wound healing, Lancet 358 (9291) (2001) 1445–1448.
[51] Z. Zhang, W. Li, D. Chang, Z. Wei, E. Wang, J. Yu, Y. Xu, Y. Que, Y. Chen, C. Fan, B. Ma, Y. Zhou, Z. Huan, C. Yang, F. Guo, J. Chang, A combination therapy for androgenic alopecia based on quercetin and zinc/copper dual-doped mesoporous silica nanocomposite microneedle patch, Bioact. Mater. 24 (2023) 81–95.
[52] S. Selvaraj, S. Krishnaswamy, V. Devashya, S. Sethuraman, U.M. Krishnan, Flavonoid-metal ion complexes: a novel class of therapeutic agents, Med. Res. Rev. 34 (4) (2014) 677–702.
[53] H. Zhang, W. Ma, H. Ma, C. Qin, J. Chen, C. Wu, Spindle-like zinc silicate nanoparticles accelerating innervated and vascularized skin burn wound healing, Adv. Healthcare Mater. 11 (10) (2022) 2102359.
[54] F. Bao, G. Pei, Z. Wu, H. Zhuang, Z. Zhang, Z. Huan, C. Wu, J. Chang, Bioactive self-pumping composite wound dressings with micropore array modified janus membrane for enhanced diabetic wound healing, Adv. Funct. Mater. 30 (49) (2020) 2005422.
[55] L. Sheng, Z. Zhang, Y. Zhang, E. Wang, B. Ma, Q. Xu, L. Ma, M. Zhang, G. Pei, J. Chang, A novel "hot spring"-mimetic hydrogel with excellent angiogenic properties for chronic wound healing, Biomaterials 264 (2021) 120414.
[56] R. Maitra, I.L. Shamovsky, W. Wang, M. Solc, G. Lawrance, S.M. Dostaler, G. M. Ross, R.J. Riopelle, Differential effects of transition metal cations on the conformation and biological activities of nerve growth factor, Neurotox. Res. 2 (4) (2000) 321–341.
[57] A.V. Aganov, D.S. Guseva, D.G. Zverev, N.I. Silkin, V.G. Shtyrlin, Y.A. Chelyshev, Cu(II) content in the structures of the peripheral nervous system at their damage, Appl. Magn. Reson. 30 (2) (2006) 201–206.
[58] J.X. Ma, J. Liu, H.L. Yu, Q. Wang, Y. Chen, L.B. Xiang, Curcumin promotes nerve regeneration and functional recovery in rat model of nerve crush injury, Neurosci. Lett. 547 (2013) 26–31.
[59] Z.W. Zhao, X.L. Li, Q. Li, Curcumin accelerates the repair of sciatic nerve injury in rats through reducing Schwann cells apoptosis and promoting myelinization, Biomed. Pharmacother. 92 (2017) 1103–1110.
[60] M. Caillaud, B. Chantemargue, L. Richard, L. Vignaud, F. Favreau, P.A. Faye, P. Vignoles, F. Sturtz, P. Trouillas, J.M. Vallat, A. Desmouliere, F. Billet, Local low dose curcumin treatment improves functional recovery and remyelination in a rat

model of sciatic nerve crush through inhibition of oxidative stress, Neuropharmacology 139 (2018) 98–116.
[61] L. Pickart, The human tri-peptide GHK and tissue remodeling, J. Biomater. Sci. Polym. Ed. 19 (8) (2008) 969–988.
[62] L. Pickart, A. Margolina, Regenerative and protective actions of the GHK-Cu peptide in the light of the new gene data, Int. J. Mol. Sci. 19 (7) (2018) 1987.